Mohsen Dadfarnia
Department of Mechanical Science and Engineering,
University of Illinois at Urbana-Champaign,
1206 West Green Street,
Urbana, IL 61801

Brian P. Somerday
Sandia National Laboratories,
P.O. Box 969,
MS 9403,
Livermore, CA 94551

Petros Sofronis[1]
Department of Mechanical Science and Engineering,
University of Illinois at Urbana-Champaign,
1206 West Green Street,
Urbana, IL 61801
e-mail: sofronis@uiuc.edu

Ian M. Robertson
Department of Material Science and Engineering,
University of Illinois at Urbana-Champaign,
1304 West Green Street,
Urbana, IL 61801

Douglas Stalheim
DGS Metallurgical Solutions, Inc.,
16110 NE 4th Street,
Vancouver, WA 98684

Interaction of Hydrogen Transport and Material Elastoplasticity in Pipeline Steels

The technology of large scale hydrogen transmission from central production facilities to refueling stations and stationary power sites is at present undeveloped. Among the problems that confront the implementation of this technology is the deleterious effect of hydrogen on structural material properties, in particular, at gas pressures of the order of 15 MPa, which are the suggested magnitudes by economic studies for efficient transport. In order to understand the hydrogen embrittlement conditions of the pipeline materials, we simulate hydrogen diffusion through the surfaces of an axial crack on the internal wall of a vessel coupled with material deformation under plane strain small scale yielding conditions. The calculation of the hydrogen accumulation ahead of the crack tip accounts for stress-driven transient diffusion of hydrogen and trapping at microstructural defects whose density evolves dynamically with deformation. The results are analyzed to correlate for a given material system the time after which hydrogen transport takes place under steady state conditions with the level of load in terms of the applied stress intensity factor at the crack tip and the size of the domain used for the simulation of the diffusion.
[DOI: 10.1115/1.3027497]

Keywords: hydrogen embrittlement, diffusion, plasticity, low- or medium-strength steels, pipeline

1 Introduction

This work addresses the interaction of hydrogen with the stress field of a crack under conditions that simulate hydrogen transport through the faces of an axial crack on the interior wall of a pipeline steel. We investigate this interaction for medium- or low-strength ferritic steels (<700 MPa) since such strength levels are dictated by safety issues, low cost considerations, and the use of these materials in the existing natural gas pipeline system (e.g., steels X42 and X52), which may also be used for hydrogen transport in the future.

The deleterious effect of hydrogen on the mechanical response of iron and steel alloys was reviewed by Hirth [1] 28 years ago. In the presence of hydrogen, materials fail at very low load levels relative to those they can sustain in the absence of hydrogen (e.g., see Refs. [1,2]). It was previously thought that hydrogen embrittlement occurs only in high-strength steels, with the effect becoming weaker at lower strengths. For high strengths (>1000 MPa), the effect is indeed weaker as the strength decreases. However, this correlation between strength and hydrogen-induced degradation does not imply that medium- or low-strength steels exhibit reduced or minimal embrittlement susceptibility. Research has shown that low- to medium-strength steels, depending on their composition and microstructure, are also susceptible to hydrogen embrittlement [3–7].

Hydrogen transport is one of the important aspects of hydrogen embrittlement. Hydrogen atoms after adsorption and absorption move through the lattice to the sites where degradation occurs. As Birnbaum [8] pointed out, the ductility dependence on temperature and strain rate, the incubation period, and the critical hydrogen concentration buildup before fracture reflect the hydrogen transport kinetics rather than the mechanisms of failure. Therefore, the analysis of the hydrogen transport processes is an essential prerequisite to any attempt to address the issue of hydrogen embrittlement related failure [9].

The first attempt to couple nonlinear diffusion phenomena with elastoplastic deformation ahead of a crack tip was made by Kitagawa and Kojima [10]. Considering drift due to hydrostatic stress and trapping generated by plastic deformation, Sofronis and McMeeking [11] studied transient diffusion of hydrogen and hydrogen trapping at microstructural defects in iron and steel in the area around a blunting crack tip. Lufrano and Sofronis [12] extended the model of Sofronis and McMeeking by including the effect of hydrogen-induced dilatation on the material constitutive model, and analyzed the interaction of hydrogen with local plasticity at cracked and round-notched geometries. In systems with large hydrogen solubility, e.g., niobium, the dilatational effect of hydrogen becomes important at high hydrogen concentrations as it affects both the stress relaxation and the diffusion paths. Krom et al. [13] extended the model of Sofronis and McMeeking by introducing a strain rate factor in the diffusion equation to accurately account for the hydrogen balance in normal interstitial lattice sites (NILS) and trapping sites. This strain rate factor is particularly important in transient calculations of hydrogen at high strain rates. Using this modified transport model, Taha and Sofronis [14] investigated the interaction between hydrostatic stress, plastic strain, and hydrogen concentration and its dependence on strength and strain rate in both high and low solubility systems. By accounting for the

[1]Corresponding author.

Contributed by the Pressure Vessel and Piping Division of ASME for publication in the JOURNAL OF PRESSURE VESSEL TECHNOLOGY. Manuscript received June 27, 2007; final manuscript received June 24, 2008; published online July 1, 2009. Review conducted by Poh-Sang Lam. Paper presented at the 2006 ASME International Mechanical Engineering Congress (IMECE2006), Chicago, IL, November 5–10, 2006.

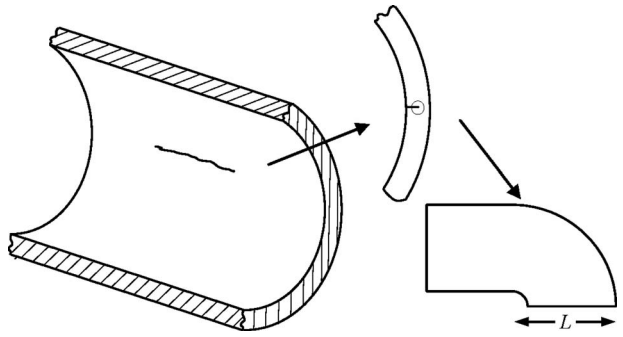

Fig. 1 Schematic of an axial crack on the ID surface of a pipeline and the crack tip region under consideration. The parameter *L* denotes the size of the analysis domain.

hydrogen effect on the flow stress and the cohesive properties of internal material interfaces and grain boundaries, Liang and Sofronis [15–17] investigated the dependence of material failure on the hydrogen transport kinetics in nickel-base alloy 690. The interaction of hydrogen transport with material atomic cohesion ahead of a crack tip was investigated recently by Serebrinsky et al. [18].

In the studies to date that address coupling of hydrogen trapping and stress-driven hydrogen diffusion, the relevant initial/boundary-value problem was solved with a uniform nonzero initial hydrogen concentration throughout the material before loading [11]. This type of initial condition applies to hydrogen transport in specimens that are first hydrogen charged and then loaded. In the case of hydrogen embrittlement of high-pressure hydrogen pipelines, hydrogen uptake occurs through the interior wall and may be accelerated by the presence of stress and deformation fields around a flaw either on the internal- or the external-surface wall. To investigate hydrogen transport under conditions simulating hydrogen uptake through the surfaces of a crack on the inner diameter (ID) surface of a pipeline (see Fig. 1), we consider a cracked domain under load, which is hydrogen free before hydrogen begins to diffuse through the crack faces. We analyze the coupling of hydrogen transport and material elastoplasticity at the crack tip under small scale yielding (SSY) conditions and room temperature. Thus, the load on the outer boundary of the domain is expressed in terms of the stress intensity factor (Fig. 2(*a*)) experienced by the crack tip due to the high hydrogen-gas pressure or due to structural loads the pipeline carries. We assume zero prescribed hydrogen concentration along this outer boundary (Fig. 2(*b*)) of the SSY domain. Although such an assumption is compatible with the trend of hydrogen to outgas through the outer diameter (OD) surface of a pipeline, its zero value is not accurate because in actuality nonzero hydrogen concentrations varying with position prevail throughout the *K*-dominated region around a crack tip in a real-world pipeline. On the other hand, we expect the development of the hydrogen concentration profiles in the fracture process zone ahead of the crack tip to be independent of the magnitude and location of the remote concentration boundary condition. This is due to the fact that hydrogen diffusion in the fracture process zone is driven by the local hydrostatic stress gradients in the neighborhood of the crack and the steep concentration gradients set by the hydrogen concentration boundary condition on the crack faces. Thus a zero remote hydrogen concentration boundary condition coupled with a SSY approach offers an expedient way to the study of hydrogen transport around pipeline cracks. Our study will yield the transient hydrogen concentration development ahead of the crack tip in terms of the material parameters, domain size, and hydrogen-gas pressure characteristics. At the same time, the numerical predictions for the time the system takes to reach steady state should be viewed as a lower bound to the actual time because of the assumed zero remote concentration boundary condition. Our initial attempt to address this problem is described in our earlier work [19,20].

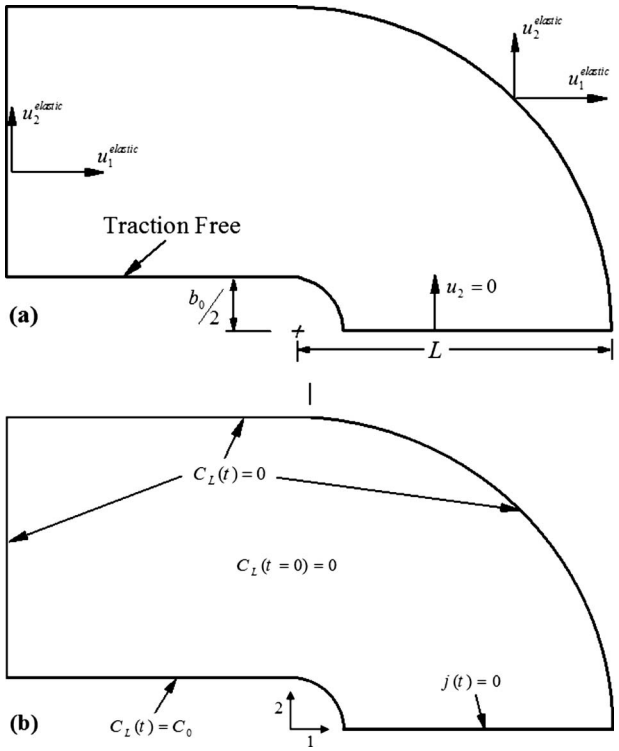

Fig. 2 Description of (*a*) boundary conditions for the elastoplastic problem and (*b*) initial and boundary conditions for the diffusion problem at the blunting crack tip. The parameter b_0 denotes the crack tip opening displacement at the undeformed state, and $u_1^{elastic}$ and $u_2^{elastic}$ are the asymptotic displacements of Irwin's singular field [24] in 1- and 2-directions, respectively. The parameter C_0 is the NILS hydrogen concentration at the crack face in equilibrium with the hydrogen gas inside the crack and *j* is the hydrogen flux.

The remainder of this paper is organized as follows: The system description and mathematical modeling issues of the coupled hydrogen diffusion and elastoplastic problem are explained in Secs. 2 and 3. Numerical results for diffusion of hydrogen under small scale yielding conditions are presented at different levels of applied stress intensity factor. A scaling of the steady state hydrogen concentration profile with the applied loads is identified. This result is used for the calculation of the time it takes for the hydrogen profiles to reach steady state in terms of the diffusion domain size.

2 Problem Statement

The hydrogen transport model [9] and the constitutive description of the material in the presence of hydrogen [16] are first briefly reviewed. It is shown that the hydrogen transport is fully coupled with material elastoplastic deformation through the hydrogen-induced dilatation [21] and the hydrogen effect on the material flow characteristics [22].

2.1 Hydrogen Transport. Hydrogen is assumed to reside either at NILS or reversible trapping sites at microstructural defects such as internal interfaces or dislocations generated by plastic deformation [11]. The two populations are always in equilibrium according to Oriani's theory [23] such that

$$\frac{\theta_T}{1-\theta_T} = \frac{\theta_L}{1-\theta_L}\exp\left(\frac{W_B}{RT}\right) \tag{1}$$

where θ_L is the occupancy of the interstitial sites, θ_T is the occupancy of the trapping sites, W_B is the trap binding energy, R

$=8.314$ J/mol K is the universal gas constant, and T is the absolute temperature. The hydrogen concentration in trapping sites C_T, measured in hydrogen atoms per unit volume, can be written as

$$C_T = \theta_T \alpha N_T \tag{2}$$

where α denotes the number of sites per trap and $N_T = N_T(\varepsilon^p)$ denotes the trap density in number of traps per unit volume as a function of the amount of the local plastic strain ε^p. The hydrogen concentration C_L in NILS, measured in hydrogen atoms per unit volume, can be phrased as

$$C_L = \theta_L \beta N_L \tag{3}$$

where β denotes the number of NILS per solvent atom and N_L denotes the number of solvent atoms per unit volume given by $N_L = N_A / V_M$, with $N_A = 6.0232 \times 10^{23}$ atoms per mole being Avogadro's number and V_M the molar volume of the host lattice measured in units of volume per mole.

The governing equation for transient hydrogen diffusion accounting for trapping and hydrostatic drift is given by [11]

$$\frac{D}{D_{\text{eff}}}\frac{dC_L}{dt} + \alpha\theta_T \frac{dN_T}{d\varepsilon^p}\frac{d\varepsilon^p}{dt} - DC_{L,ii} + \left(\frac{DV_{\text{H}}}{3RT} C_L \sigma_{kk,i}\right)_{,i} = 0 \tag{4}$$

and the concentration at trapping sites is calculated through Eqs. (1)–(3) as

$$C_T = \frac{K_T \alpha N_T C_L}{\beta N_L + (K_T - 1) C_L} \tag{5}$$

In these equations, $(\,)_{,i} = \partial(\,)/\partial x_i$, d/dt is the time derivative, D is the hydrogen diffusion coefficient through NILS, D_{eff} is an effective diffusion coefficient given by

$$\frac{D_{\text{eff}}}{D} = \left(1 + \frac{\partial C_T}{\partial C_L}\right)^{-1} = \left(1 + \frac{K_T \alpha \beta N_L N_T}{[\beta N_L + (K_T - 1) C_L]^2}\right)^{-1} \tag{6}$$

V_{H} is the partial molar volume of hydrogen in solid solution, σ_{ij} is the Cauchy stress, $K_T = \exp(W_B/RT)$ is the equilibrium constant, and a repeated index implies the standard summation convention over the range. Equation (4) shows that in order to calculate the hydrogen distribution within a solid, one should solve a coupled problem of hydrogen diffusion and elastoplasticity. Oriani's model assumes that the trap filling kinetics is very rapid. Consequently, the effective diffusion coefficient D_{eff} is less than the normal NILS diffusion coefficient D as long as the traps are not saturated or as new traps are created by plastic straining.

2.2 Elastoplastic Deformation in the Presence of Hydrogen. The material is assumed to be linearly elastic and isotropic with moduli and flow stress independent of the local hydrogen concentration. In the plastic regime, the material hardens isotropically and flows according to von Mises J_2 flow theory. The associated flow rule for plastic loading is given by

$$\overset{\nabla}{\sigma}_{ij} = 2G\left(\delta_{ik}\delta_{jl} + \frac{\nu}{1-2\nu}\delta_{ij}\delta_{kl} - \frac{3\sigma'_{ij}\sigma'_{kl}}{2\left(\frac{h}{3G}+1\right)\sigma_e^{\,2}}\right)(D_{kl} - D^{\text{H}}_{kl}) \tag{7}$$

whereas for elastic loading or any unloading

$$\overset{\nabla}{\sigma}_{ij} = 2G\left(\delta_{ik}\delta_{jl} + \frac{\nu}{1-2\nu}\delta_{ij}\delta_{kl}\right)(D_{kl} - D^{\text{H}}_{kl}) \tag{8}$$

where D_{ij} denotes the total deformation rate tensor that equals the symmetric part of the velocity gradient in spatial coordinates, δ_{ij} is the Kronecker delta, the superposed ∇ denotes the Jaumann stress rate, $\sigma'_{ij} = \sigma_{ij} - (\sigma_{kk}/3)\delta_{ij}$ is the deviatoric stress, $\sigma_e = \sqrt{3\sigma'_{ij}\sigma'_{ij}/2}$ is the equivalent stress, G and ν are the shear modulus and Poisson's ratio, respectively, and $h = d\sigma/d\varepsilon^p$ is the slope of the uniaxial Cauchy stress versus logarithmic plastic strain ε^p curve. In multiaxial deformation, ε^p is calculated through $\varepsilon^p = \sqrt{2D^p_{ij}D^p_{ij}/3}$. The total deformation rate tensor D_{ij} is decomposed as

$$D_{ij} = D^e_{ij} + D^p_{ij} + D^{\text{H}}_{ij} \tag{9}$$

where D^e_{ij}, D^p_{ij}, and D^{H}_{ij} denote, respectively, the elastic, plastic, and hydrogen parts. The mechanical effect of the hydrogen solute atoms is purely dilatational [21] and is phrased in terms of the deformation rate as

$$D^{\text{H}}_{ij} = \frac{d}{dt}\left[\ln\left(1 + \frac{(c - c_0)\Delta v}{3\Omega}\right)\right]\delta_{ij} \tag{10}$$

where c is the total hydrogen concentration measured in hydrogen atoms per solvent atom, c_0 is the initial hydrogen concentration in the stress free lattice, $\Delta v = V_{\text{H}}/N_A$ is the volume increase per hydrogen atom introduced into solution, and Ω is the mean atomic volume of the host metal atom.

Equations (4)–(10) indicate that the hydrogen diffusion initial/boundary-value problem and the elastic-plastic boundary problem are coupled [11]. The finite element procedures for the solution of the coupled problems are outlined in the works by Sofronis and McMeeking [11] and Liang and Sofronis [16].

3 Numerical Results for Hydrogen-Gas Pressure of 1 atm

The initial/boundary-value problem of hydrogen diffusion coupled with material elastoplasticity was solved near a blunting crack tip with an initial opening displacement $b_0 = 1$ μm. Plane strain conditions were considered as the analysis is concerned with an ID surface crack along the axial direction (Fig. 1). We assumed that the plastic zone size is small compared with the pipeline wall thickness and therefore we used the boundary approach of small scale yielding under mode I opening. The asymptotic displacements of the Irwin singular linear elastic field [24] were imposed on the outer boundary of the domain of analysis located at a distance L from the crack tip (Fig. 2(a)). We note that the domain size, which is smaller than the thickness of the pipeline, sets along with the diffusion coefficient the time scale of the problem. Figure 2(b) shows the hydrogen-related boundary and initial conditions of the problem. The outer surface is assigned a zero concentration boundary condition, i.e., $C_L = 0$, and the axis of symmetry ahead of the crack tip a zero flux, i.e., $j = 0$. For the first series of calculations, we considered a domain size $L = 9.79$ mm and a gas pressure of 1 atm. Thus on the crack surface, the NILS hydrogen concentration C_L is assumed to be in equilibration with the hydrogen gas of 1 atm at all times, i.e., $C_L = C_0 = 2.084 \times 10^{21}$ H atoms/m^3 ($=2.46 \times 10^{-8}$ H atoms per solvent atoms). The system's temperature is 300 K. Different domain sizes L and crack surface concentrations C_L in equilibrium with higher gas pressure were also investigated, and the relevant results are reported in Sec. 4. The chosen shape of the outer boundary shown in Fig. 2 allowed for convenient and very fine element discretization of the part of the domain close to the crack face. Such fine discretization was required for the treatment of the steep concentration gradients set by the imposed hydrogen-concentration boundary condition at the crack face.

At time zero, we assume that there is no hydrogen in the material. We apply the displacements on the remote boundary incrementally at a constant stress intensity factor rate toward a final value K_I. After loading, and while the load is held constant at K_I, we switch on hydrogen diffusion through the crack faces. It should be mentioned that T-stress effects on the interaction of hydrogen with the material microstructure ahead of a crack tip are also important, in particular, in the case of shallow cracked specimens as Liang et al. [25] have found. The interaction of the T-stress with the hydrogen transport under the boundary conditions outlined in Fig. 2(a) is the subject of another investigation [26,27].

Table 1 Material properties

Properties	Symbol	Value
Young's modulus	E	201.88 GPa
Poisson's ratio	ν	0.3
Yield stress	σ_0	595 MPa
Work hardening exponent	n	0.059
No. of sites per trap	α	1
No. of NILS per host atom	β	1
Trap binding energy	W_B	60 kJ/mol [28]
Molar volume of the host lattice	V_M	7.116 cm^3/mol
Partial molar volume of H	V_H	2 cm^3/mol [1]
Diffusion coefficient	D	2×10^{-8} m^2/s [1]
Volume change per H atom	$\Delta v/\Omega$	0.281 [1]
Solubility at a temperature of 300 K	K	0.005434 mol $H_2/m^3\sqrt{MPa}$ [1]

The material used in the simulations is a new X70/X80 type of an acicular ferrite pipeline microstructure whose mechanical properties are given in Table 1. The uniaxial stress-strain curve has been measured experimentally and is approximated by a power-law relationship of the form $\sigma_e=\sigma_0(1+\varepsilon^p/\varepsilon_0)^n$, where ε^p is the plastic strain and $\varepsilon_0=\sigma_0/E$. The trap density N_T is assumed to increase with plastic straining according to the experimental results of Kumnick and Johnson [28] who also found a trap binding energy of 60 kJ/mol.

Figures 3 and 4 show, respectively, contour plots of normalized hydrostatic stress and plastic strain at a stress intensity factor $K_I=30$ MPa $\sqrt{m}$. The corresponding crack tip opening displacement b defined by the 90 deg intersection method is equal to 4.62 μm, more than four times the initial crack tip opening displacement b_0. As can be seen from Fig. 4, the plastic zone is confined to the crack tip in agreement with the small scale yielding assumption.

The distribution of hydrogen concentration reaches a steady state after 2 h and 53 min, where time $t=0$ corresponds to the switching on of the hydrogen diffusion. The contour plots of the

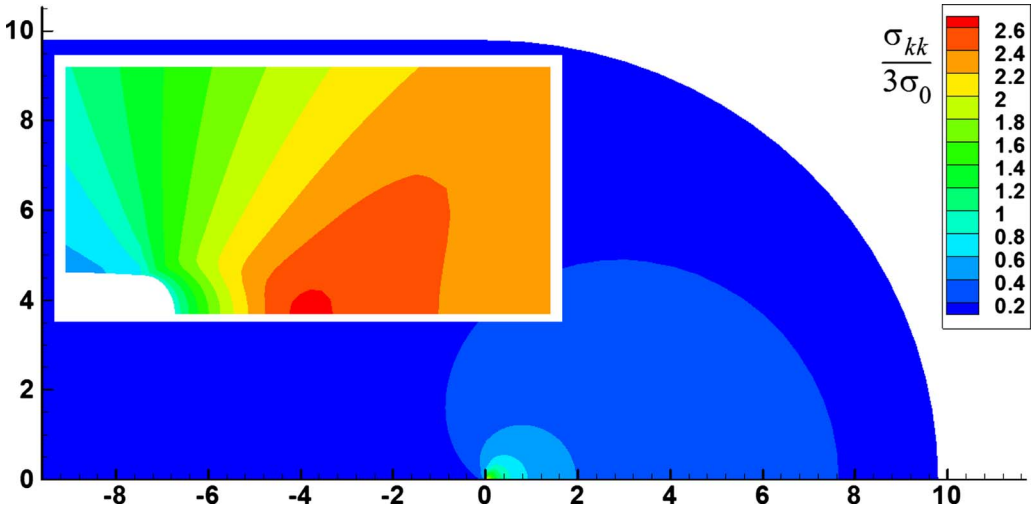

Fig. 3 Contour plots of normalized hydrostatic stress $\sigma_{kk}/3\sigma_0$ at applied stress intensity factor $K_I=30$ MPa $\sqrt{m}$. The parameter σ_0 denotes the yield stress of the material, and the inset shows the hydrostatic stress near the notch root. Dimensions are in millimeters.

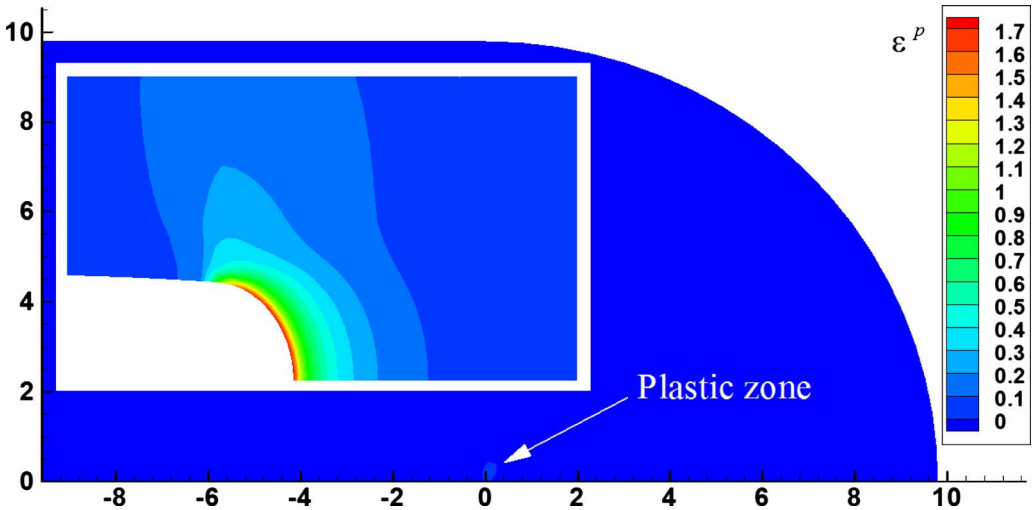

Fig. 4 Contour plots of equivalent plastic strain ε^p at applied stress intensity factor $K_I=30$ MPa $\sqrt{m}$. The inset shows the equivalent plastic strain near the notch root and dimensions are in millimeters.

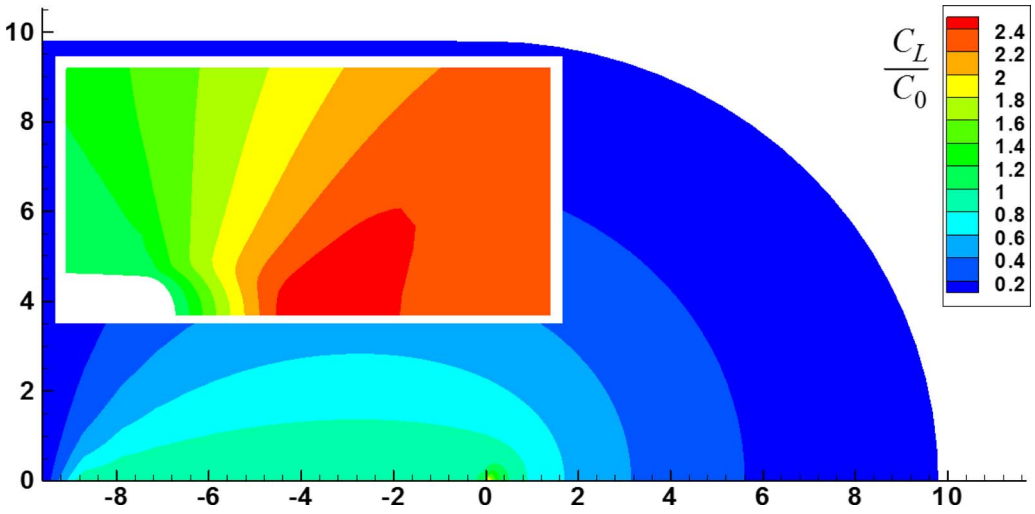

Fig. 5 Contour plots of normalized NILS hydrogen concentration C_L/C_0 at steady state under K_I =30 MPa $\sqrt{\text{m}}$. The inset shows the concentration near the notch root. The parameter $C_0=2.084\times10^{21}$ H atoms/m^3 (=2.46×10^{-8} H atoms per solvent atoms) is the enforced NILS hydrogen concentration at the crack face in equilibrium with a hydrogen-gas pressure of 1 atm.

hydrogen field parameters at steady state under K_I=30 MPa $\sqrt{\text{m}}$ are shown in Figs. 5–7. Figure 5 shows the normalized NILS concentration C_L/C_0. The distribution of C_L near the notch root varies in accordance with the hydrostatic stress (inset of Fig. 3). The equivalent plastic strain attains its peak value at the crack tip and rapidly decreases at distances away from the tip. Thus, as Fig. 6 shows, the site of accumulation of trapped hydrogen is near the crack surface, and the profile of the trapped concentration C_T follows closely that of the plastic strain (Fig. 4). This is because the trap density increases monotonically with plastic strain [28]. Figure 7 shows the normalized total hydrogen concentration ahead of the notch, which is essentially governed by the trapped hydrogen populations (Fig. 6); the magnitude of the NILS concentration (Fig. 5) is much smaller than that of the trapped hydrogen (Fig. 6).

Figure 8 shows the normalized concentration C_L/C_0 in NILS along the axis of symmetry ahead of the notch against normalized distance R/b from the notch root in the undeformed configuration as time elapses toward steady state. The parameter b denotes the current crack tip opening displacement at K_I=30 MPa $\sqrt{\text{m}}$. The effect of hydrostatic stress on configuring the steady state hydrogen concentration profile in NILS can be clearly seen in this figure.

The shape of the NILS concentration profile is dictated by several processes. At early times, the high value of the hydrogen concentration gradient at the crack surface forces hydrogen to diffuse into the specimen. At the root of the crack notch, the trapping sites generated by plastic straining demand for hydrogen. At the same time, hydrogen is attracted to the hydrostatic peak location inside from the root. Due to the large trap binding energy, trapping sites are filled up quickly depleting hydrogen from the NILS. After the trapping sites are saturated, hydrostatic stress gradients pull hydrogen away from the crack tip toward the hydro-

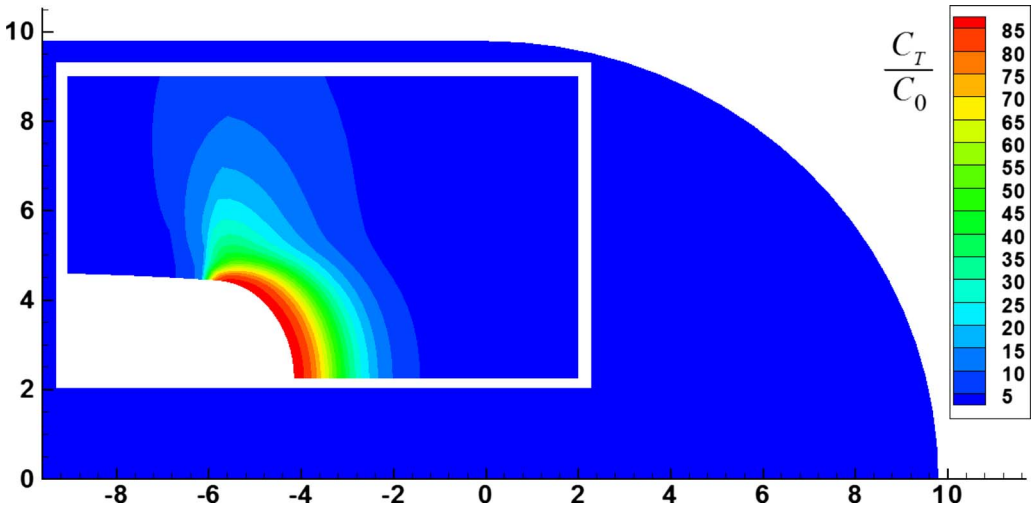

Fig. 6 Contour plots of normalized trapping site hydrogen concentration C_T/C_0 at steady state under K_I=30 MPa $\sqrt{\text{m}}$. The inset shows the concentration at the notch root. The parameter $C_0=2.084\times10^{21}$ H atoms/m^3 (=2.46×10^{-8} H atoms per solvent atoms) is the enforced NILS hydrogen concentration at the crack face in equilibrium with a hydrogen-gas pressure of 1 atm.

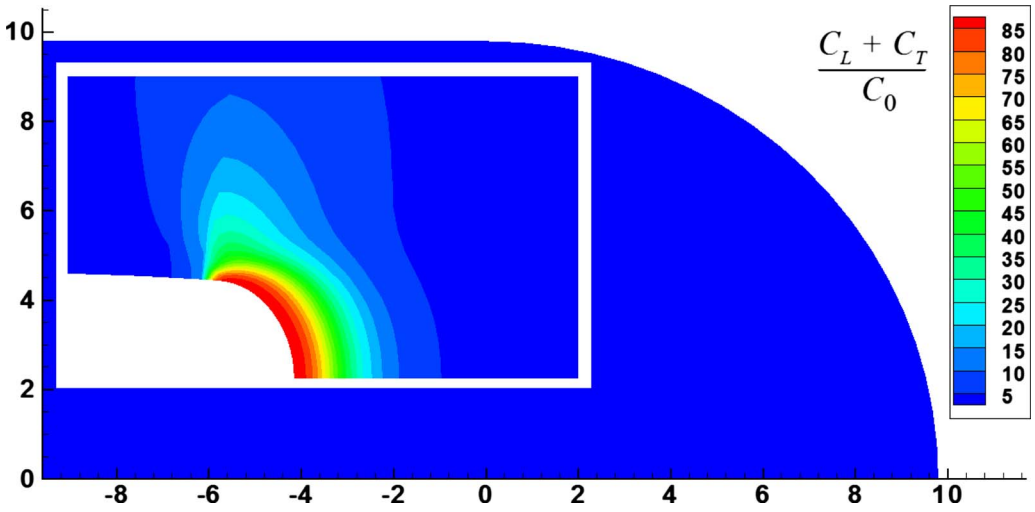

Fig. 7 Contour plots of total hydrogen concentration $(C_L+C_T)/C_0$ at steady state under K_I =30 MPa $\sqrt{m}$. The inset shows the hydrogen concentration at the notch root. The parameter C_0 =2.084×10^{21} H atoms/m^3 (=2.46×10^{-8} H atoms per solvent atoms) is the enforced NILS hydrogen concentration at the crack face in equilibrium with a hydrogen-gas pressure of 1 atm.

static stress-peak location, and this creates a local peak in the NILS hydrogen concentration. These processes along with the fact that the concentration C_L at the crack surface is kept constant at the value C_0 at all times determine the shape of the C_L concentration profiles shown in Fig. 8.

At this point we introduce a parameter t_{ss} that we term an effective time to steady state and use it to denote the time at which the NILS hydrogen concentration at the stress-peak location reaches 98% of its final steady state value. Practically the effective time to steady state describes the time at which steady state in the fracture process zone has almost been reached while in the rest of the specimen diffusion to steady state continues on. This effective

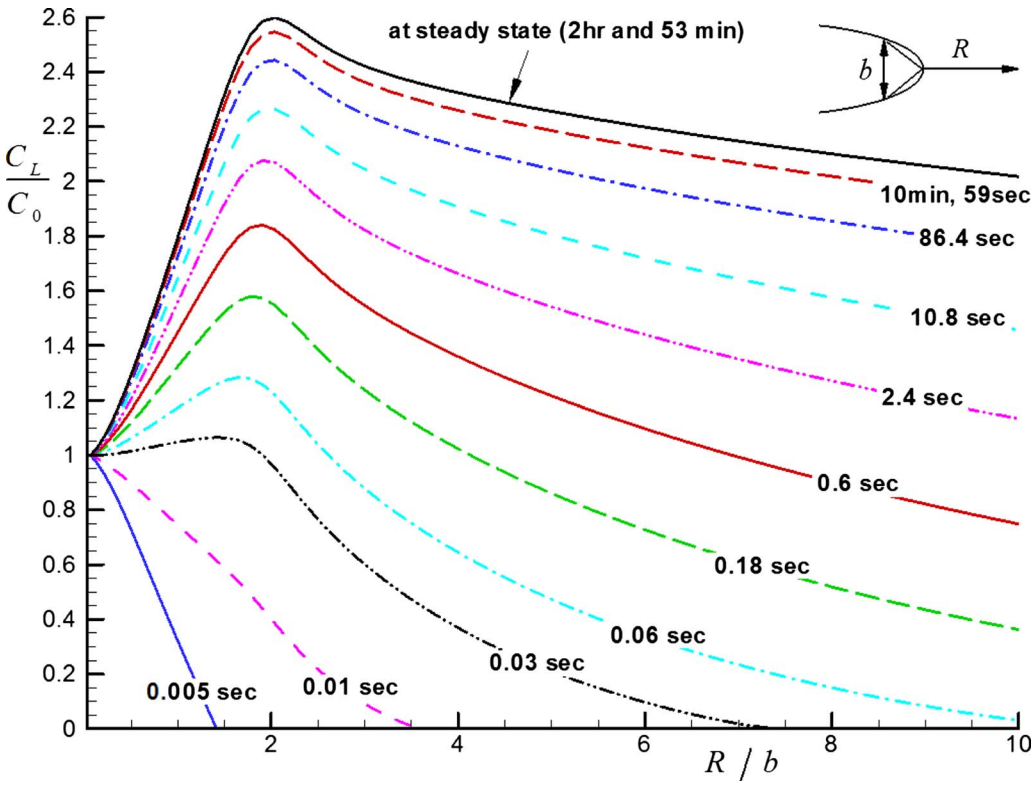

Fig. 8 Evolution of normalized hydrogen concentration C_L/C_0 in NILS versus normalized distance R/b ahead of the crack tip at K_I=30 MPa $\sqrt{m}$ with a domain size L=9.79 mm. The parameter b =4.62 μm denotes the crack tip opening displacement and C_0=2.084×10^{21} H atoms/m^3 (=2.46×10^{-8} H atoms per solvent atoms) is the enforced NILS hydrogen concentration at the crack face in equilibrium with a hydrogen-gas pressure of 1 atm.

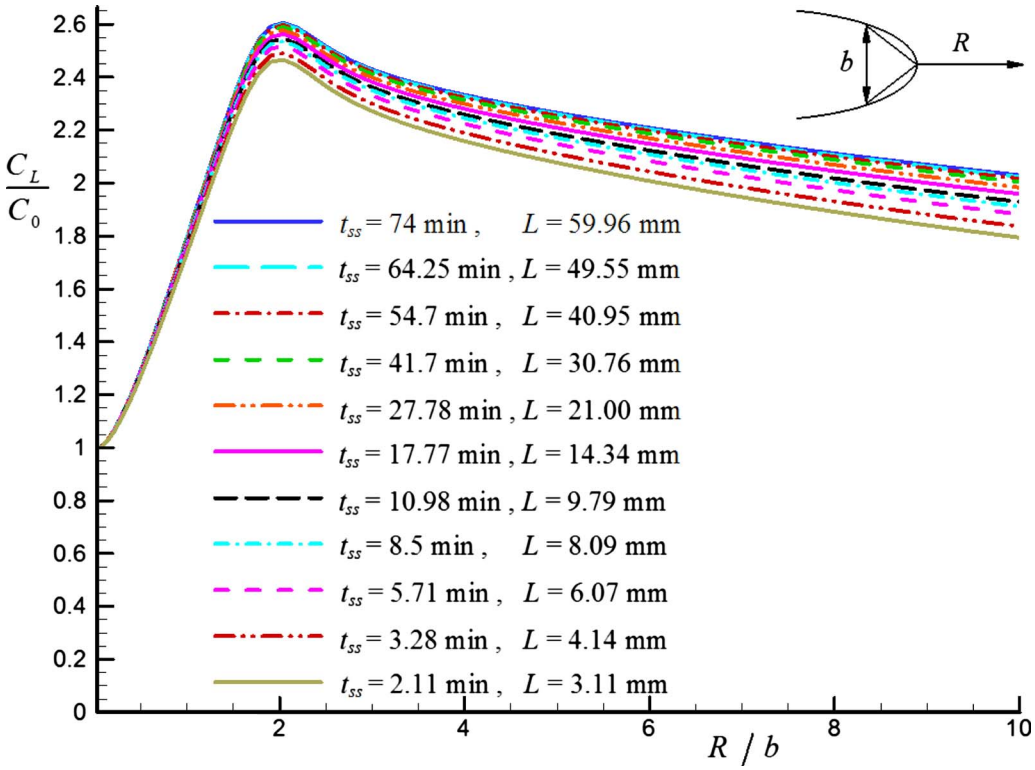

Fig. 9 Normalized NILS hydrogen concentration C_L/C_0 at $t=t_{ss}$ (effective time to steady state) versus normalized distance R/b ahead of the crack tip at $K_I=30$ MPa $\sqrt{m}$ for various domain sizes. The parameter $C_0=2.084\times10^{21}$ H atoms/m^3 ($=2.46\times10^{-8}$ H atoms per solvent atoms) is the enforced NILS hydrogen concentration at the crack face in equilibrium with a hydrogen-gas pressure of 1 atm.

steady state time may be correlated with a bound to the time required for the hydrogen degradation effect to occur. For the applied stress intensity factor $K_I=30$ MPa $\sqrt{m}$, the material/geometric parameters, and the initial/boundary conditions we used in the simulations, t_{ss} is equal to 10 min and 59 s, as shown in Fig. 8.

To examine the effect of the domain size L on the steady state concentration profiles and time t_{ss}, we performed additional transient hydrogen transport calculations with $L=3.11$, 4.14, 6.07, 8.09, 9.79, 14.34, 20.01, 30.76, 40.95, 49.55, and 59.96 mm under stress intensity factor $K_I=30$ MPa $\sqrt{m}$. For these domain sizes, t_{ss} values were found to be 2.11 min, 3.28 min, 5.71 min, 8.5 min, 10.98 min, 17.77 min, 27.78 min, 41.7 min, 54.7 min, 64.25 min, and 74 min, respectively. The corresponding NILS concentrations at time t_{ss} are plotted in Fig. 9. As the domain size gets larger, the peak value of the NILS concentration increases. However, Fig. 10 shows that as the domain size increases the normalized peak val-

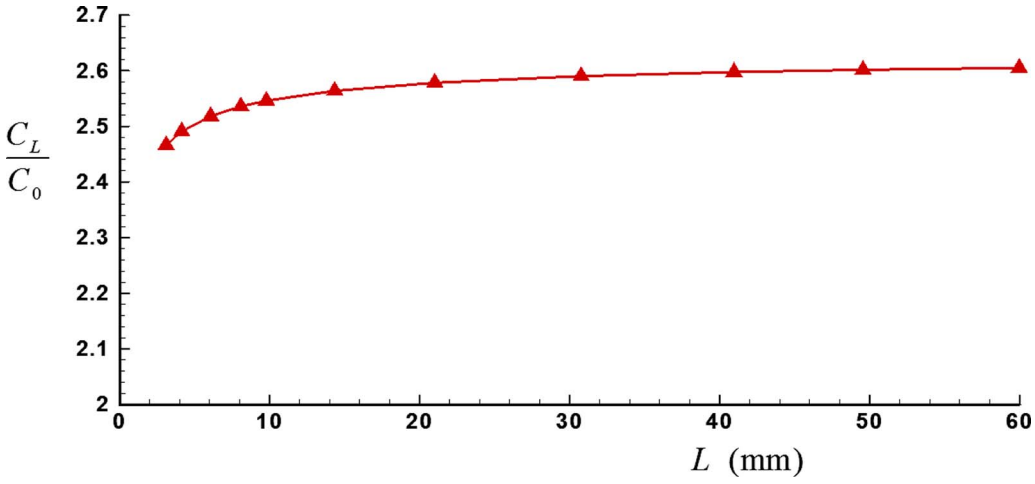

Fig. 10 Plot of peak values of the normalized hydrogen concentration C_L/C_0 in NILS at $t=t_{ss}$ (effective time to steady state) versus domain size L at $K_I=30$ MPa $\sqrt{m}$. The parameter $C_0=2.084\times10^{21}$ H atoms/m^3 ($=2.46\times10^{-8}$ H atoms per solvent atoms) is the enforced NILS hydrogen concentration at the crack face in equilibrium with a hydrogen-gas pressure of 1 atm.

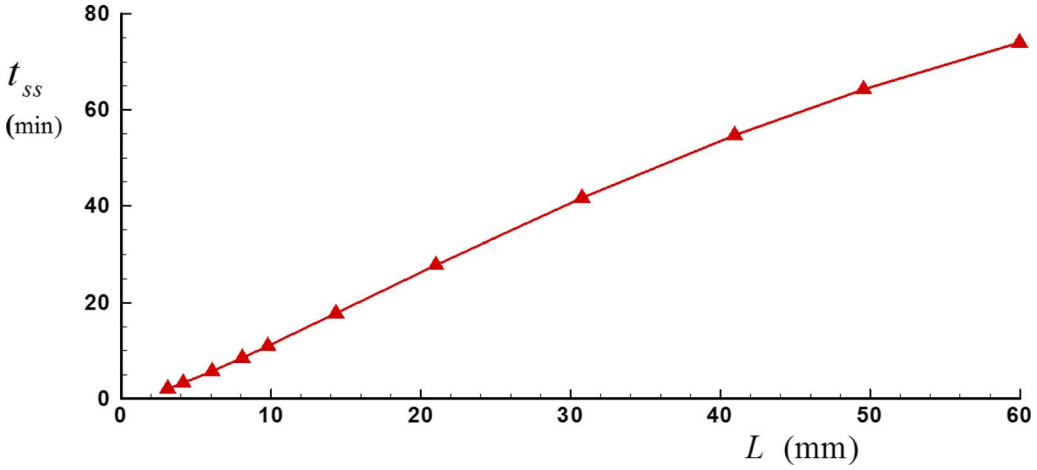

Fig. 11 Plot of effective time to steady state t_{ss} versus domain size L at K_I=30 MPa $\sqrt{m}$. The crack face is in equilibrium with hydrogen gas at 1 atm pressure.

ues of the NILS concentration at t_{ss} tend to level at a value about 2.6. The time to steady state t_{ss} as a function of the domain size is shown in Fig. 11. The plot shows nearly a linear relationship between t_{ss} and domain size in the range of 3–60 mm domain size.

In order to investigate the effect of the magnitude of the applied load on the evolution of the hydrogen concentration profiles, additional simulations were carried out at a different applied stress intensity factor K_I. Specifically, K_I=80 MPa $\sqrt{m}$ was used with an initial crack tip opening displacement b_0=6 μm and an associated current crack tip opening displacement b=31.77 μm. For domain sizes L=14.34, 20.01, 30.76, 40.95, 49.55, 59.96, and 79.82 mm the effective times to steady state t_{ss} were found to be 52.6 min, 96.8 min, 173.5 min, 266.4 min, 341.3 min, 432 min, and 590.4 min, respectively. As in Figs. 10 and 11, the peak values of NILS concentration at t_{ss} and the time to steady state t_{ss} for various domain sizes are plotted in Figs. 12 and 13, respectively. The effective time to steady state t_{ss} exhibits nearly a linear relationship with the domain size in the range of 14–80 mm for a given stress intensity factor (Figs. 11 and 13).

4 Discussion

The effect of the stress intensity factor on the results can be understood better by looking at the nondimensionalized form of the hydrogen transport equation (4). For this, we introduce the following nondimensionalized parameters:

$$\xi_i = \frac{x_i}{b}, \quad \tau = \frac{Dt}{b^2}, \quad \phi = \frac{C_L}{C_0}, \quad \rho = \frac{\sigma_{kk} V_H}{3RT} \tag{11}$$

where b is a nondimensionalizing length taken equal to the crack tip opening displacement and C_0 is a reference hydrogen concentration taken equal to the hydrogen concentration on the ID surface of the vessel in equilibrium with hydrogen gas as dictated by Sievert's law. Substituting the nondimensionalized parameters (11) in Eq. (4), one obtains the following transport equation:

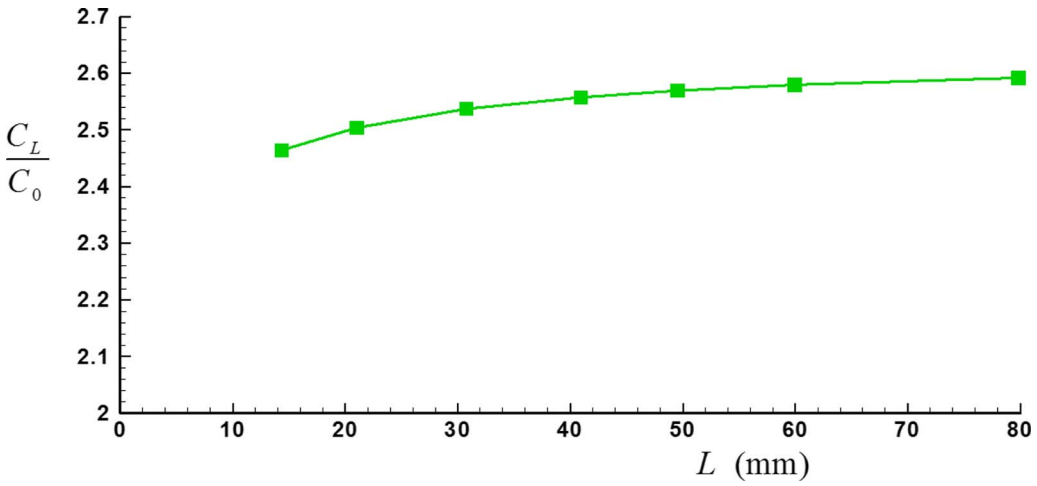

Fig. 12 Plot of peak values of the normalized hydrogen concentration C_L/C_0 in NILS at $t=t_{ss}$ (effective time to steady state) versus domain size L at K_I=80 MPa $\sqrt{m}$. The parameter C_0=2.084×10^{21} H atoms/m^3 (=2.46×10^{-8} H atoms per solvent atoms) is the enforced NILS hydrogen concentration at the crack face in equilibrium with a hydrogen-gas pressure of 1 atm.

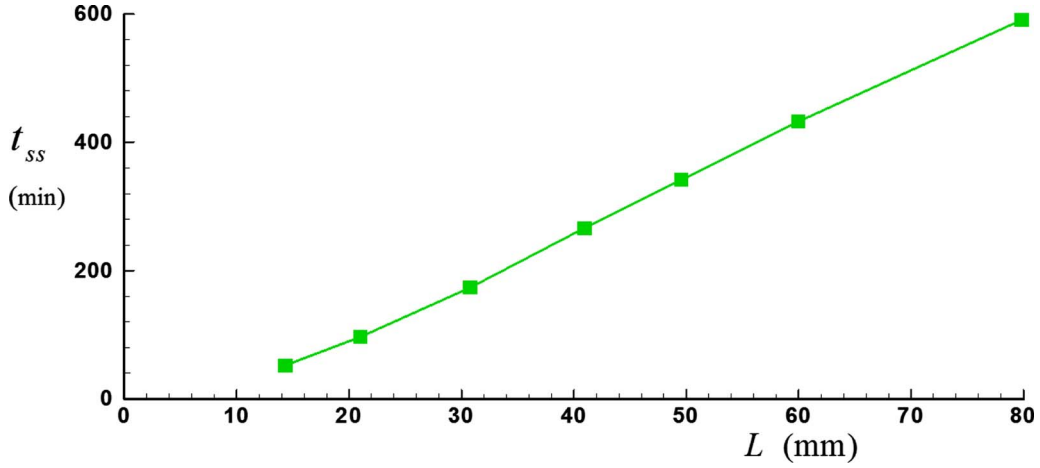

Fig. 13 Plot of effective time to steady state t_{ss} versus domain size L at K_I=80 MPa $\sqrt{m}$. The crack face is in equilibrium with hydrogen gas at 1 atm pressure.

$$\frac{D}{D_{\text{eff}}}\frac{d\phi}{d\tau}+\frac{\alpha\theta_T}{C_0}\frac{dN_T}{d\varepsilon^p}\frac{d\varepsilon^p}{d\tau}-\frac{\partial^2\phi}{\partial\xi_i\partial\xi_i}+\frac{\partial}{\partial\xi_i}\left(\phi\frac{\partial\rho}{\partial\xi_i}\right)=0 \qquad (12)$$

Note that αN_T denotes hydrogen atomic sites per unit volume and therefore the ratio $\alpha N_T/C_0$ in the second term of Eq. (12) is dimensionless. By Eq. (6), so is also D/D_{eff}.

In Eq. (12), ε^p, ρ, and consequently $\partial\rho/\partial\xi_i$ are functions of ξ_i and τ and exhibit no explicit dependence on K_I. As a result, form (12) is the same for all applied stress intensities, and the solution for the nondimensionalized concentration ϕ is a function of ξ_i and τ with no explicit dependence on K_I and L. Of course, as demonstrated in Figs. 10–13, there exists an implicit dependence of ϕ on K_I and L through the crack opening displacement b that is used to define ξ_i and due to the fact that the boundary condition ϕ=0 is enforced on the outer boundary of the domain (Fig. 2) whose distance from the notch tip is set by L. Hence, scaling of the normalized hydrogen concentrations and the true or effective time to steady state in terms of the nondimensionalized domain size L/b is warranted. The results for the maximum steady state hydrogen concentration C_L/C_0 at t_{ss}, as shown in Figs. 10 and 12 and the effective time to steady state t_{ss} as shown in Figs. 11 and 13, are replotted as functions of the normalized domain size L/b in Figs. 14 and 15, respectively. Clearly these plots do confirm our argument that the normalized hydrogen concentrations and the effective time to steady state exhibit a dependence on the domain size and the applied stress intensity factor that scales with L/b.

Figure 15 shows that the nondimensionalized effective time to steady state $\tau_{ss}=Dt_{ss}/b^2$ exhibits nearly a linear dependence on the normalized domain size L/b. Using a linear regression analysis to interpolate the numerical data of Fig. 15, one finds $t_{ss}=(0.285L-0.064b)b$ for the given diffusion coefficient 2×10^{-8} m^2/s, where t_{ss} is measured in minutes, L in millimeters, and b in microns. For the range of 10 mm$<L<$60 mm and 4.6 μm$<b<$15.0 μm and under small scale yielding conditions, the effective time to steady state for a given domain size increases monotonically with the crack tip opening displacement b, that is, with the applied stress intensity factor. Therefore, for the given range of L and b, the larger the magnitude of the applied stress intensity factor K_I, the larger the effective time t_{ss} to steady state. This is reasoned out by the fact that as the stress intensity factor increases, the hydrostatic stress-peak location moves further inside from the notch tip [29,30].

In order to investigate the effect of hydrogen pressure on the

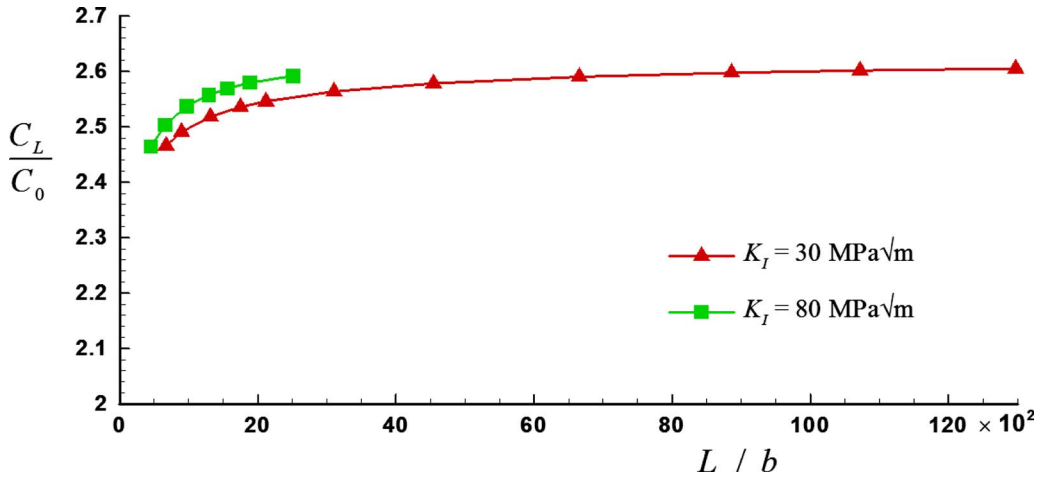

Fig. 14 Plot of peak values of the normalized hydrogen concentration C_L/C_0 in NILS at $t=t_{ss}$ (effective time to steady state) versus the normalized domain size L/b at different applied stress intensity factors. The parameter C_0=2.084×10^{21} H atoms/m^3 (=2.46×10^{-8} H atoms per solvent atoms) is the enforced NILS hydrogen concentration at the crack face in equilibrium with a hydrogen-gas pressure of 1 atm.

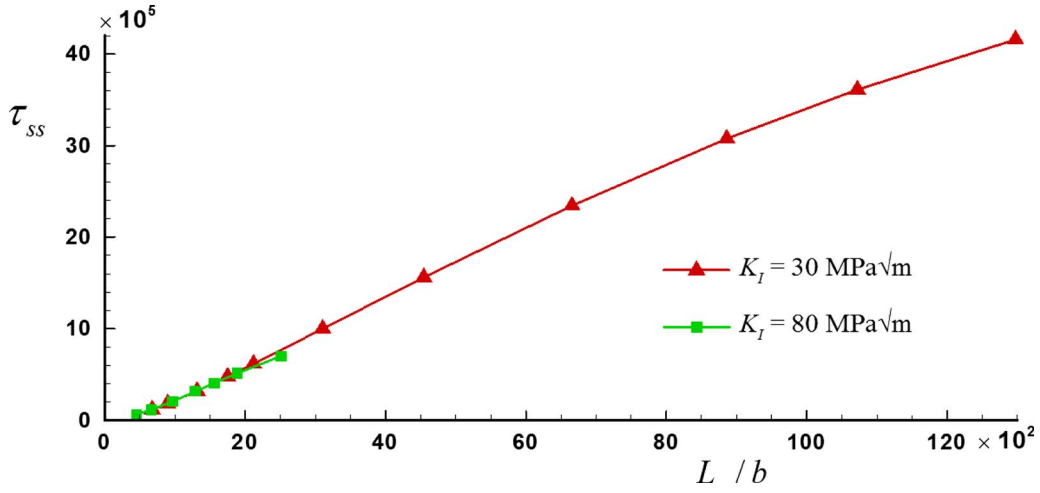

Fig. 15 Plot of the normalized effective time to steady state $\tau_{ss}=Dt_{ss}/b^2$ versus normalized domain size L/b at different applied stress intensity factors. The crack face is in equilibrium with hydrogen gas at 1 atm pressure.

magnitude of the hydrogen concentration profiles and the time to steady state, we performed additional simulations in which the hydrogen concentration on the crack faces (Fig. 2) was taken to be in equilibrium with hydrogen gas at a pressure of 15 MPa. Thus, the NILS boundary concentration condition was $C_L=C_0'=12.77C_0=2.659\times10^{22}$ H atoms/m^3 ($=3.142\times10^{-7}$ H atoms per solvent atoms). Numerical results were obtained for the same domain sizes L=3.11, 4.14, 6.07, 8.09, 9.79, 14.34, 20.01, 30.76, 40.95, 49.55, and 59.96 mm and applied stress intensity factor K_I=30 MPa $\sqrt{\text{m}}$. The corresponding values for the effective time to steady state t_{ss} were found to be 1.15 min, 1.8 min, 3.14 min, 4.68 min, 5.95 min, 9.72 min, 15.12 min, 22.5 min, 31 min, 37 min, and 43 min. For the given diffusion coefficient 2×10^{-8} m^2/s, these data are interpolated by $t_{ss}=(0.164L-0.056b)b$, where t_{ss} is measured in minutes, L in millimeters, and b in microns.

The normalized NILS concentration profiles ahead of the crack tip at time t_{ss} for various domain sizes are plotted in Fig. 16. The corresponding peak values of NILS concentration at t_{ss} are shown in Fig. 17. Comparing Figs. 9 and 16, one notices that even

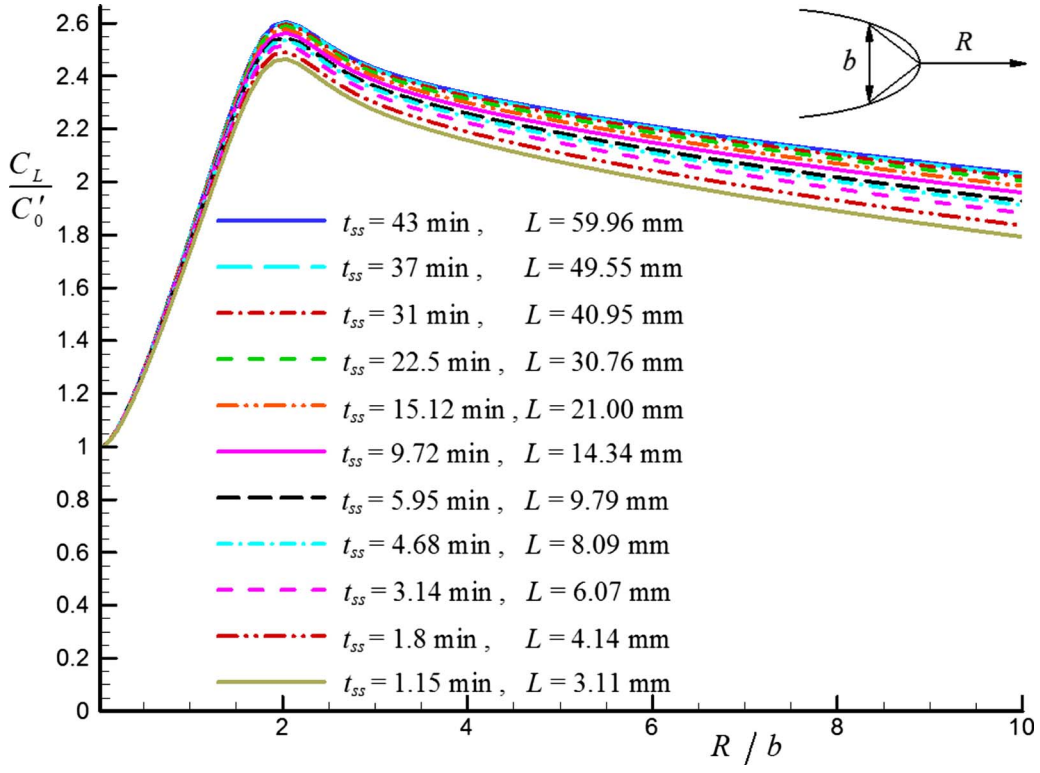

Fig. 16 Normalized hydrogen concentration C_L/C_0' in NILS at $t=t_{ss}$ (effective time to steady state) versus normalized distance R/b ahead of the crack tip for various domain sizes. The parameter $C_0'=12.77C_0$ is the enforced initial/boundary NILS hydrogen concentration at the crack face in equilibrium hydrogen gas at 15 MPa.

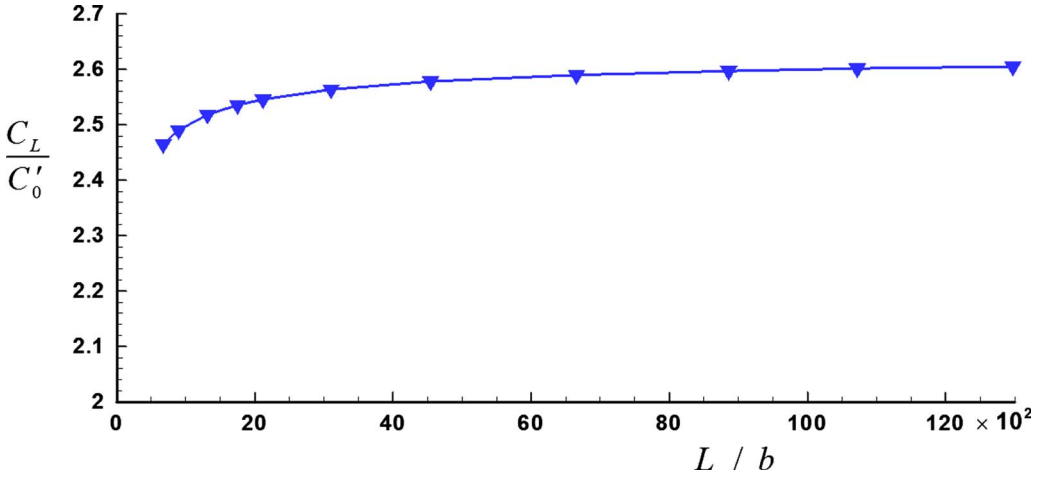

Fig. 17 Plot of peak values of the normalized hydrogen concentration in NILS at $t=t_{ss}$ (effective time to steady state) against normalized domain size L/b. The parameter $C_0'=12.77C_0$ is the enforced initial/boundary NILS hydrogen concentration at the crack face in equilibrium with hydrogen gas at 15 MPa.

though the initial hydrogen concentrations at the crack face are different, the normalized NILS hydrogen concentration profiles at t_{ss} are the same for a given domain size L. This can be explained by the steady state form of the normalized hydrogen transport equation (12):

$$-\frac{\partial^2 \phi}{\partial \xi_i \partial \xi_i}+\frac{\partial}{\partial \xi_i}\left(\phi \frac{\partial \rho}{\partial \xi_i}\right)=0 \tag{13}$$

Equation (13) shows that there is no dependence of the steady state profiles on the boundary hydrogen concentration at the crack face. However, as shown in Fig. 18, the effective time to steady state τ_{ss} does depend on the boundary crack-face concentration for any given normalized domain size. Also, the parameter τ_{ss} continues to exhibit nearly a linear dependence on the normalized domain size even for a hydrogen pressure equal to 15 MPa. The fact that τ_{ss} depends on the boundary concentration on the crack faces can be understood by looking at Eq. (6). This equation indicates that the diffusion coefficient ratio D_{eff}/D is a nonlinear function of the NILS hydrogen concentration. Therefore, since the normalized hydrogen transport equation (12) depends on this ratio, the time to steady state does involve an influence from the initial/boundary concentration condition at the crack faces.

Looking at the nondimensionalized hydrogen transport equation (12), one sees that there is no explicit dependence on the hydrogen diffusion coefficient D—the ratio D_{eff}/D is independent of D. Therefore, the effective nondimensionalized time τ_{ss} to steady state is independent of D, as shown in Eq. (6). Then by virtue of the definition of the nondimensionalized time τ through Eq. (11) and noting that the parameter τ_{ss} is not an explicit function of the applied stress intensity factor (Fig. 15), one concludes that

$$t_{ss}=\frac{b^2}{D}\tau_{ss}(L/b,\ \text{initial/boundary concentration, material parameters}) \tag{14}$$

For the material parameters used in the present calculations, the functional dependence of τ_{ss} on its arguments is presented in Fig. 18 for various values of L/b and crack-face concentrations of $C_0=2.084\times10^{21}$ H atoms/m^3 and $C_0'=12.77C_0$. The importance of Eq. (14) lies on the fact that it represents a scaling of the time to steady state with the hydrogen diffusion coefficient through NILS. For instance, if the domain geometry, the magnitude of the load, and all material properties remain the same while the diffusion coefficient is increased by a factor of 10, the time to steady

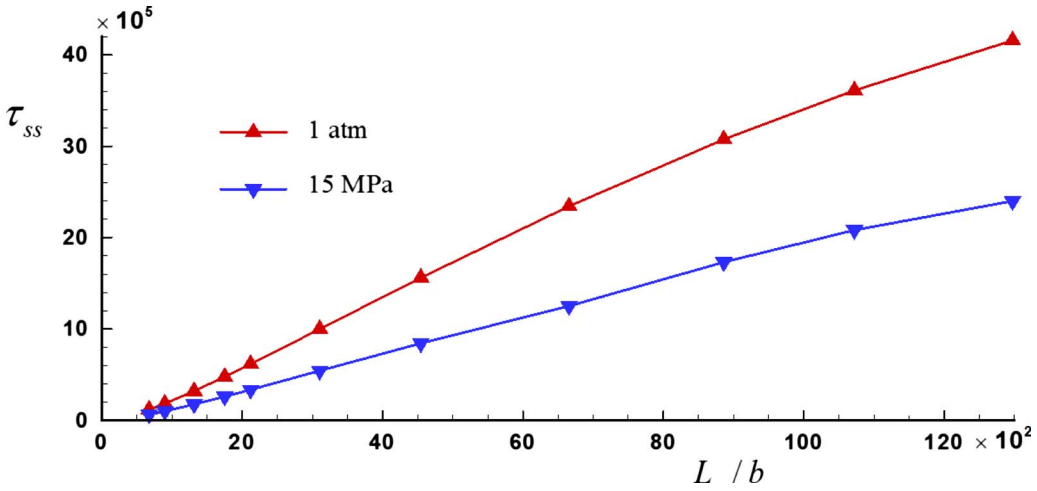

Fig. 18 Plot of the normalized effective time to steady state $\tau_{ss}=Dt_{ss}/b^2$ against normalized domain size L/b with the crack face being in equilibrium with hydrogen gas at 1 atm and 15 MPa.

state decreases by a factor of 10. This is an important result in view of the existing ambiguity around the magnitude of the diffusion coefficient in bcc ferritic systems. Because of the extensive trapping in these steels, a large range of diffusivities have been reported around room temperature [31]. According to the present calculations, one only needs to compute the time to steady state for just one value of the diffusion coefficient.

The present results were obtained under the assumption of SSY conditions ahead of a crack tip. For this assumption to be valid, the plastic zone size should be much smaller than the wall thickness h of the pipeline. This dictates that our present results pertain to pipelines for which the wall thickness h is of the same order of magnitude as the domain size L we used in our SSY analysis, that is, $L \sim h$. A hydrogen pressure of 6.89 MPa (1000 psi) induces a crack tip stress intensity of 12.36 MPa $\sqrt{\text{m}}$ [32] at an axial crack of length h and depth $0.2h$. The plastic zone size for this crack is $r_p=(1/3\pi)(K/\sigma_0)^2=0.033$ mm and this is certainly much smaller than 10.0 mm, which represents a realistic pipeline thickness. Similarly, for the same crack, a hydrogen pressure of 13.78 MPa (2000 psi) induces a stress intensity of 24.72 MPa $\sqrt{\text{m}}$ with a corresponding plastic zone size of 0.131 mm. Certainly, we may argue that the extent of the stress and strain fields for these two cases does meet the SSY requirement.

With regard to the transient profiles toward steady state, Eq. (12) indicates that the nondimensionalized time for any distribution of nondimensionalized hydrogen concentration to be developed ahead of the crack tip before hydrogen begins to outgas through the outer boundary is nearly independent of the domain size. For example, under a hydrogen pressure of 1 atm, the value of (C_L/C_0) at the peak location reaches 2.4 at about $\tau=44{,}000$, which corresponds to an actual time of about 47 s when the applied stress intensity factor is 30 MPa $\sqrt{\text{m}}$ ($b=4.62$ μm). The point here is that if degradation takes place before hydrogen begins to outgas through the outer boundary and requires a critical hydrogen concentration, SSY analysis can be used to predict the time of the occurrence of the event.

The issues related to the location and the magnitude of the remote concentration boundary condition and the conditions on hydrogen pressure and wall thickness for which K-dominance is indeed prevalent ahead of a crack tip in a real-world pipeline need further investigation. Resolution of these issues related to the interaction of hydrogen diffusion and material elastoplasticity requires an analysis of the response of the entire pipeline cross section in the presence of an axial crack [26,27].

5 Concluding Remarks

The coupled transient hydrogen diffusion initial/boundary-value problem and the large strain elastoplastic boundary-value problem were solved under small scale yielding conditions in the neighborhood of a blunting crack tip exposed to a hydrogen gas environment using material properties for an X70/80 type steel. An effective time parameter t_{ss} for hydrogen diffusion to reach steady state was introduced. It denotes the time at which the NILS hydrogen concentration at the hydrostatic-stress-peak location reaches 98% of the final steady state value. The effective time has been defined in terms of the transients of the diffusible hydrogen, which configures the NILS populations. Once the NILS populations reach steady state so do the corresponding trapping ones, as dictated in Eq. (1). The simulation results obtained under small scale yielding conditions may be summarized as follows:

(i) The effective time to steady state t_{ss} is inversely proportional to the diffusion coefficient D as described in Eq. (14) for a given material system and domain size.
(ii) For the domain size in the range of 10–60 mm and applied stress intensity factor in the range of 30–55 MPa $\sqrt{\text{m}}$, the effective time to steady state for a given domain size increases monotonically with increasing stress intensity factor for pressures up to 15 MPa. Specifically, for the material data used in the present work, $t_{ss}=(0.285L-0.064b)b$ for a hydrogen pressure of 1 atm and $t_{ss}=(0.164L-0.056b)b$ for a hydrogen pressure of 15 MPa, where t_{ss} is measured in minutes, L in millimeters, and the crack opening displacement b in microns.
(iii) The magnitude of the peak NILS concentration at steady state and the effective time to steady state scale with the nondimensionalized domain size L/b, where b is the crack tip opening displacement.
(iv) The magnitude of the normalized peak NILS concentration at steady state seems to level to a value less than 2.70 as the normalized domain size L/b increases.
(v) The nondimensional effective time $\tau_{ss}=Dt_{ss}/b^2$ varies almost linearly with the normalized domain size L/b and depends on the hydrogen-gas pressure as Fig. 18 indicates. In particular, the nondimensionalized time for any distribution of nondimensionalized hydrogen concentration to be attained ahead of the crack tip before steady state is nearly independent of the domain size.
(vi) Given that a real-world pipeline thickness is of the order of 10 mm, the small scale yielding assumption for an axial crack with depth equal to 2.0 mm is expected to be valid for pressures up to 15.0 MPa.

Since the local amounts of hydrogen in the fracture process zone along with the local values of the stress and deformation fields control any possible hydrogen-induced degradation, we expect that the calculated time to steady state provides a measure of the time for the embrittlement of a vessel. Of course experimental evidence is required to discern the importance of hydrogen at NILS or trapping sites on the triggering of the degradation effect. Precise identification of the embrittlement conditions requires the coupling of the present simulations with a micromechanics model for fracture. Experimental work and theoretical calculations of fracture initiation ahead of a crack tip is the subject of ongoing research. In particular, permeation measurements are used to determine the trapping and diffusion characteristics of the alloy X70/X80 we studied in this investigation.

Acknowledgment

The authors gratefully acknowledge support from U.S. Department of Energy contract (Grant No. GO15045), the Sandia National Laboratories under U.S. Department of Energy Contract No. DE-AC04-94AL85000, and the National Science Foundation (Grant DMR 0302470). Also the authors would like to acknowledge discussions at the beginning of this work with Dr. G. Muralidharan of the Oak Ridge National Laboratory.

Nomenclature

b = crack tip opening displacement in the deformed state
b_0 = crack tip opening displacement in the undeformed state
C_0 = hydrogen concentration in interstitial sites at the crack face under 1 atm pressure measured in atoms per m^3
C_L = hydrogen concentration in interstitial sites measured in atoms per m^3
C_T = hydrogen concentration in trapping sites measured in atoms per m^3
c = total hydrogen concentration measured in hydrogen atom per solvent atom
c_0 = hydrogen concentration at the crack face under 1 atm pressure measured in atoms per solution atom
D = hydrogen diffusion coefficient through interstitial sites

D_{eff} = effective hydrogen diffusion coefficient
D_{ij}^{e} = elastic part of deformation rate tensor
D_{ij}^{p} = plastic part of deformation rate tensor
D_{ij}^{H} = deformation rate tensor for lattice straining due to hydrogen
D_{ij} = total deformation rate $=D_{ij}^{e}+D_{ij}^{p}+D_{ij}^{\text{H}}$
E = Young's modulus
G = shear modulus
h = slope of uniaxial Cauchy stress versus logarithmic plastic strain
K = solubility of hydrogen in steel
K_I = stress intensity factor
K_T = equilibrium constant
L = domain size
N_A = Avogadro's number
N_L = number of solvent atoms per unit volume
N_T = trap density
n = work hardening coefficient
R = universal gas constant
T = temperature
t = time
t_{ss} = effective time to steady state
V_{H} = partial molar volume of hydrogen
V_M = molar volume of the host lattice
W_B = trap binding energy
x_i = coordinate system
α = number of sites per trap
β = number of NILS per host atom
δ_{ij} = Kronecker delta
Δv = volume increase per hydrogen atom $=V_{\text{H}}/N_A$
ε_0 = yield strain
ε^p = equivalent plastic strain
θ_L = occupancy of the interstitial sites
θ_T = occupancy of the trapping sites
ν = Poisson's ratio
ξ_i = nondimensional coordinate $=x_i/b$
ρ = nondimensional hydrostatic stress $=\sigma_{kk}V_{\text{H}}/3RT$
σ_0 = yield stress
σ_e = equivalent stress
σ_{ij} = Cauchy's stress
σ'_{ij} = deviatoric stress
$\overset{\nabla}{\sigma}_{ij}$ = Jaumann rate of stress
Ω = mean atomic volume of the host lattice
τ = nondimensional time $=Dt/b^2$
ϕ = nondimensional NILS concentration $=C_L/C_0$

References

[1] Hirth, J. P., 1980, "Effect of Hydrogen on the Properties of Iron and Steel," Metall. Trans. A, **11**, pp. 861–890.
[2] Birnbaum, H. K., Robertson, I. M., Sofronis, P., and Teter, D., 1997, "Mechanisms of Hydrogen Related Fracture—A Review," *Second International Conference on Corrosion Deformation Interactions, CDI'96*, Nice, France, Sept. 24–26, 1996, T. Magnin, ed., The Institute of Materials, Great Britain, pp. 172–195.
[3] Thompson, A. W., 1977, "Materials for Hydrogen Service," *Hydrogen: Its Technology and Implications*, Transmission and Storage, Vol. 2, K. E. Cox and K. D. Williamson, eds., CRC, Cleveland, OH, pp. 85–124.
[4] Lee, T. D., Goldenberg, T., and Hirth, J. P., 1979, "Effect of Hydrogen on Fracture of U-Notched Bend Specimens of Spheroidized AISI 1095 Steel," Metall. Trans. A, **10**(4), pp. 199–208.
[5] Onyewuenyi, O. A., and Hirth, J. P., 1983, "Effects of Hydrogen on Notch Ductility and Fracture in Spheroidized AISI 1090 Steel," Metall. Trans. A, **14**(2), pp. 259–269.
[6] Robinson, S. L., and Stoltz, R. E., 1981, "Toughness Losses and Fracture Behavior of Low Strength Carbon-Manganese Steels in Hydrogen," *Hydrogen Effects in Metals*, I. M. Bernstein and A. W. Thompson, eds., The Metallurgical Society of AIME, Warrendale, PA, pp. 987–995.
[7] Cialone, H. J., and Holbrook, J. H., 1988, "Sensitivity of Steels to Degradation in Gaseous Hydrogen," *Hydrogen Embrittlement: Prevention and Control*, (ASTM STP 962), L. Raymond, ed., American Society for Testing and Materials, Philadelphia, PA, pp. 134–152.
[8] Birnbaum, H. K., 1977, "Hydrogen Related Failure Mechanisms in Metals," *Environmental Sensitive Fracture of Engineering Materials, Proceedings of Symposium on Environmental Effects on Fracture*, Chicago, IL, Oct. 24–26, Z. A. Foroulis, ed., Metallurgical Society of AIME, Warendale, PA, pp. 326–360.
[9] Birnbaum, H. K., and Sofronis, P., 1994, "Hydrogen-Enhanced Localized Plasticity—A Mechanism for Hydrogen Related Fracture," Mater. Sci. Eng., A, **176**, pp. 191–202.
[10] Kitagawa, H., and Kojima, Y., 1983, "Diffusion of Hydrogen Near an Elastoplastically Deformed Crack Tip," *Atomistic Fracture, Proceedings of a NATO Advanced Research Institute on Atomistics of Fracture*, Calcatoggio, Corsica, France, May 22–31 1981, R. A. Latanision and J. R. Pickens, eds., Plenum, New York, pp. 799–811.
[11] Sofronis, P., and McMeeking, R. M., 1989, "Numerical Analysis of Hydrogen Transport Near a Blunting Crack Tip," J. Mech. Phys. Solids, **37**(3), pp. 317–350.
[12] Lufrano, J., and Sofronis, P., 1999, "Enhanced Hydrogen Concentration Ahead of Rounded Notches and Cracks—Competition Between Plastic Strain and Hydrogen Stress," Acta Mater., **46**(5), pp. 1519–1526.
[13] Krom, A. H. M., Koers, R. W. J., and Bakker, A., 1999, "Hydrogen Transport Near a Blunting Crack Tip," J. Mech. Phys. Solids, **47**(4), pp. 971–992.
[14] Taha, A., and Sofronis, P., 2001, "A Micromechanics Approach to the Study of Hydrogen Transport and Embrittlement," Eng. Fract. Mech., **68**(6), pp. 803–837.
[15] Liang, Y., and Sofronis, P., 2001, "Toward a Phenomenological Description of Hydrogen-Induced Decohesion at Particle/Matrix Interfaces," J. Mech. Phys. Solids, **51**, pp. 1509–1531.
[16] Liang, Y., and Sofronis, P., 2003, "Micromechanics and Numerical Modeling of the Hydrogen-Particle-Matrix Interactions in Nickel-Base Alloys," Modell. Simul. Mater. Sci. Eng., **11**, pp. 523–551.
[17] Liang, Y., and Sofronis, P., 2004, "On Hydrogen-Induced Void Nucleation and Grain Boundary Decohesion in Nickel-Base Alloys," ASME J. Eng. Mater. Technol., **126**, pp. 368–377.
[18] Serebrinsky, S., Carter, E. A., and Ortiz, M., 2004, "A Quantum-Mechanically Informed Continuum Model of Hydrogen Embrittlement," J. Mech. Phys. Solids, **52**, pp. 2403–2430.
[19] Dadfarnia, M., Sofronis, P., Robertson, I. M., Somerday, B. P., Muralidharan, G., and Stalheim, D., 2006, "Numerical Simulation of Hydrogen Transport at a Crack Tip in a Pipeline Steel," *Proceedings of the Biennial International Pipeline Conference, IPC*, Calgary, AB, Canada, pp. 193–199. Sept. 25–29, Paper No. IPC2006-102007.
[20] Dadfarnia, M., Sofronis, P., Robertson, I. M., Somerday, B. P., Muralidharan, G., and Stalheim, D., 2006, "Micromechanics of Hydrogen Transport and Embrittlement in Pipeline Steels," *2006 ASME International Mechanical Engineering Congress and Exposition*, Chicago IL, Nov. 5–10, Paper No. IMECE 2006-16325.
[21] Peisl, H., 1978, "Lattice Strains Due to Hydrogen in Metals," *Hydrogen in Metals I*, (*Topics in Applied Physics* Vol. 28), G. Alefeld and J. Volkl, eds., Springer-Verlag, New York, pp. 53–74.
[22] Robertson, I. M., 2001, "The Effect of Hydrogen on Dislocation Dynamics," Eng. Fract. Mech., **68**(6), pp. 671–692.
[23] Oriani, R. A., 1970, "The Diffusion and Trapping of Hydrogen in Steel," Acta Metall., **18**(1), pp. 147–157.
[24] Irwin, G. R., 1960, "Fracture Mechanics," *Structural Mechanics, Proceedings of the First Symposium of Naval Structural Mechanics*, J. N. Goodier and N. J. Hoff, eds., Stanford University, pp. 557–594.
[25] Liang, Y., Sofronis, P., and Dodds, R. H., Jr., 2004, "Interaction of Hydrogen With Crack-Tip Plasticity: Effects of Constraint on Void Growth," Mater. Sci. Eng., A, **366**(2), pp. 397–411.
[26] Dadfarnia, M., Sofronis, P., Robertson, I. M., and Somerday, B. P., 2007, "Hydrogen/Plasticity Interaction at Internal Cracks in Pipeline Steels," *Seventh International ASTM/ESIS Symposium on Fatigue and Fracture*, Tampa, FL, Nov.
[27] Dadfarnia, M., Sofronis, P., Somerday, B. P., and Robertson, I. M., 2008, "On the Small Scale Character of the Stress and Hydrogen Concentration Fields at the Tip of an Axial Crack in Steel Pipeline: Effect of Hydrogen-Induced Softening on Void Growth," Int. J. Mater. Res., **99**(5), pp. 557–570.
[28] Kumnick, A. J., and Johnson, H. H., 1980, "Deep Trapping States for Hydrogen in Deformed Iron," Acta Metall., **28**(1), pp. 33–39.
[29] Rice, J. R., and Johnson, M. A., 1970, "The Role of Large Crack Tip Geometry Changes in Plane Strain Fracture," *Inelastic Behavior of Solids*, M. F. Kanninen, W. F. Adler, A. R. Rosenfield, and R. I. Jaffee, eds., McGraw-Hill, New York, pp. 641–672.
[30] McMeeking, R. M., 1977, "Finite Deformation Analysis of Crack-Tip Opening in Elastic-Plastic Materials and Implications for Fracture," J. Mech. Phys. Solids, **25**, pp. 357–381.
[31] Völkl, J., and Alefeld, G., 1978, "Diffusion of Hydrogen in Metals," *Hydrogen in Metals I*, (*Topics in Applied Physics* Vol. 28), G. Alefeld and J. Volkl, eds., Springer-Verlag, New York, pp. 53–74.
[32] Raju, I. S., and Newman, J. C., Jr., 1982, "Stress-Intensity Factors for Internal and External Surface Cracks in Cylindrical Vessels," ASME J. Pressure Vessel Technol., **104**(4), pp. 293–299.